Virologica Sinica 41 (2026) 700–710

Contents lists available at ScienceDirect

Virologica Sinica

journal homepage: www.keaipublishing.com/en/journals/virologica-sinica
www.virosin.org

Research Article

Bruton's tyrosine kinase inhibitor BTKi-2 inhibits mpox virus and vaccinia virus infection

Chen Yang [a,1], Runchu Zhao [b,1], Shuting Huo [a,1], Yaqing Zhang [a], Jingxi Feng [a], Mingli Gong [a,2], Lin Zhu [c], Conggang Zhang [d], Linqi Zhang [a], Jing Xue [c], Rong Zhang [e], Qihui Wang [b], Qiang Ding [a,*]

[a] School of Basic Medical Sciences, Tsinghua University, Beijing 100084, China
[b] CAS Key Laboratory of Pathogen Microbiology and Immunology, Institute of Microbiology, Chinese Academy of Sciences, Beijing 100101, China
[c] Institute of Laboratory Animals Science, CAMS & PUMC, Beijing 100021, China
[d] School of Pharmaceutical Sciences, Tsinghua University, Beijing 100084, China
[e] School of Basic Medical Sciences, Shanghai Medical College, Fudan University, Shanghai 200433, China

ARTICLE INFO

Keywords:
Mpox virus (MPXV)
Vaccinia virus (VACV)
High-content screening
BTK inhibitor-2
EGFR
ERBB2

ABSTRACT

The recent global outbreak of mpox virus (MPXV) infections underscores the urgent need for antiviral therapies against orthopoxviruses. In this study, using a high-content screening (HCS) platform based on a modified vaccinia virus Tiantan strain with GFP insertion (MVTT-GFP) under BSL-2 conditions, we screened 1513 kinase inhibitors for antiviral activity. Among these, Bruton's tyrosine kinase inhibitor BTKi-2 emerged as a potent candidate, exhibiting IC_{50} of 0.535 μM against vaccinia virus (VACV) and 0.260 μM against MPXV *in vitro*, while maintaining low cytotoxicity. In a murine model of VACV-induced pneumonia, BTKi-2 treatment reduced lung viral loads by 90% and a significantly improved survival compared to vehicle-treated controls. Notably, mechanistic studies indicate that BTKi-2's antiviral effects cannot be completely attributed to the inhibition of BTK or EGFR/ErbB2 signaling. These findings highlight BTKi-2 as a promising antiviral agent *in vitro* and *in vivo*, suggesting that BTKi-2 may offer a potential avenue for future therapeutic development against orthopoxvirus infections.

INTRODUCTION

The global mpox landscape has continued to evolve since the 2022 clade IIb outbreak, which caused more than 100,000 confirmed cases across over 120 countries and continues to circulate at low levels (Minhaj, 2022; Mitjà et al., 2023; Titanji et al., 2024; Tiwari et al., 2025; Wu et al., 2025). In parallel, outbreaks of clade I MPXV, particularly clade Ib, have expanded in Central and Eastern Africa since late 2023 and have been associated with exported cases and community transmission outside Africa (Ndembi et al., 2025; Pérez-García et al., 2026; Vakaniaki et al., 2024). Although WHO lifted the 2024 mpox Public Health Emergency of International Concern in September 2025, mpox remains a public health threat, with continued risk of flare-ups and new outbreaks requiring sustained surveillance and response capacity (Taylor, 2025).

Current antiviral therapeutic options for MPXV include antibody-based therapies and small-molecule inhibitors. Although antibody therapies such as vaccinia immune globulin intravenous (VIGIV) (De Clercq et al., 2023) and monoclonal antibodies targeting viral surface proteins (VACV A33, B5, A27, and MPXV M1) have demonstrated broad cross-neutralizing activity (Gilchuk et al., 2016), their high cost and limited availability restrict widespread use. Among clinically-used small

* Corresponding author.
E-mail address: qding@tsinghua.edu.cn (Q. Ding).
Peer review under the responsibility of editorial board of *Virologica Sinica*.
[1] Chen Yang, Runchu Zhao and Shuting Huo contributed equally to this work.
[2] Present address: Mingli Gong: CAS Key Laboratory of Pathogen Microbiology and Immunology, Institute of Microbiology, Chinese Academy of Sciences, Beijing 100101, China.

https://doi.org/10.1016/j.virs.2026.06.011
Received 10 December 2025; Accepted 16 June 2026
Available online 19 June 2026

molecule antivirals, cidofovir and its prodrug brincidofovir target viral DNA replication (Foster et al., 2017), whereas tecovirimat (ST-246) inhibits F13L/VP37-mediated viral wrapping and release (Adler et al., 2022; Duraffour et al., 2015). Despite initial therapeutic promise, brincidofovir has shown limited clinical benefit in MPXV patients (Adler et al., 2022). Similarly, ST-246 was safe but did not significantly shorten the time to lesion resolution compared with placebo in randomized placebo-controlled trials in patients with mpox (The PALM007 Writing Group, 2025; Zucker et al., 2026). In addition, mutations in the viral F13L/VP37 target can confer tecovirimat resistance, with resistant viruses reported particularly in severely immunocompromised patients receiving prolonged or repeated tecovirimat treatment (Smith et al., 2023). Recent studies have therefore explored additional viral targets such as VP39 2′-O methyltransferase, E12 subunit of the mRNA cap N7-methyltransferase complex, E5 helicase–primase, H1 phosphatase, and poxin/cGAMP nuclease (Wang et al., 2026). However, most of these candidates remain at the structural, biochemical, or preclinical stage and have not yet been validated as human mpox therapies.

In light of these challenges, there is a pressing need to expand the antiviral options against orthopoxviruses (Fang et al., 2024). One promising strategy is the development of host-targeting antiviral agents (HTAs), which act on host cell factors essential for viral infection rather than on viral components directly, thereby offering a higher barrier to resistance (Karim et al., 2023). Previous studies have shown that host kinases play pivotal roles in the life cycles of various viruses (Hajjo et al., 2023; Kang et al., 2025; Keating and Striker, 2012), including MPXV (Reeves et al., 2005, 2011) and vaccinia virus (VACV), by phosphorylating viral proteins that are critical for processes such as actin-based motility. For example, Src family kinases phosphorylate the VACV protein A36R (Frischknecht et al., 1999), and the non-receptor tyrosine kinase Abl further enhances this modification (Newsome et al., 2006). These findings underscore the potential of targeting host kinases as an antiviral strategy.

Motivated by this rationale, we performed a phenotypic high-content screening (HCS) (Yang et al., 2024) using a modified vaccinia virus (Tiantan strain) engineered to express a GFP reporter (MVTT-GFP), allowing real-time visualization of infection under BSL-2 conditions. Screening a library of 1513 kinase inhibitors with this model, we identified BTKi-2 as a potent antiviral candidate. BTKi-2 inhibited VACV (IC_{50} = 0.535 μM), MPXV (IC_{50} = 0.260 μM), and ectromelia virus (ECTV) in various cell lines. Furthermore, treatment with BTKi-2 in a murine model of VACV-induced pneumonia reduced lung viral loads by approximately 90% and significantly improved the survival outcomes. However, mechanistic studies revealed that the antiviral activity of BTKi-2 is beyond BTK and EGFR/ErbB2 signaling. Collectively, these results suggest that BTKi-2 provides a novel alternative therapeutic approach for MPXV infections.

RESULTS

High-content screening using MVTT-GFP identifies BTK inhibitor-2 as a promising antiviral

Due to the biosafety level 3 (BSL-3) requirements for working with MPXV, we employed a modified vaccinia virus (Tiantan strain) with a GFP reporter gene (designated MVTT-GFP) as a surrogate model for drug discovery under BSL-2 conditions. In this system, viral infection can be directly quantified by measuring GFP positivity. We first validated the MVTT-GFP system using Huh7 cells infected with MVTT-GFP and treated with either DMSO (negative control) or ST-246 (positive control). At 24 h post-infection, HCS analysis revealed a marked difference in GFP positivity between the two groups (Fig. 1A), confirming the robustness and efficiency of this platform for antiviral screening.

Given the critical role of protein phosphorylation in the viral life cycle—and previous reports demonstrating anti-VACV activity of host-targeting kinase inhibitors such as imatinib mesylate (Gleevec) (Reeves et al., 2005, 2011) and gefitinib (IRESSA) (Langhammer et al., 2011; Mercer et al., 2010), we hypothesized that kinase inhibitors might be effective antiviral agents against poxviruses. Therefore, we screened the MedChemExpress (MCE) kinase inhibitor library containing 1513 compounds at a final concentration of 5 μM in Huh7 cells infected with MVTT-GFP. After 24 h, HCS imaging analysis was conducted to quantify cell numbers (via DAPI nuclear staining) and GFP positivity (Fig. 1B). In our controls, the DMSO-treated group consistently showed a GFP positivity rate above 80%, whereas the ST-246-treated group dropped below 20% (Fig. 1C). Z′ scores calculated from the control wells confirmed high plate quality (Zhang et al., 1999), with all plates scoring above 0.8 (criterion > 0.5) (Fig. 1D).

For each sample, infection rates and cell numbers were normalized to the corresponding DMSO control, allowing for inter-plate comparisons (Supplementary Table S1). Antiviral activity was defined by a reduction in infection rate, whereas cytotoxicity was inferred from a decrease in cell number. Apart from the positive control, ST-246 (highlighted in red, Fig. 1E), with a normalized infection rate of 18% and a normalized cell count of 110%, fifteen compounds reduced infection rates to ~20% with minimal cytotoxicity (normalized cell count > 80%, highlighted in red in Supplementary Table S1 and further evaluated in Supplementary Fig. S1). Among them, Bruton's tyrosine kinase inhibitor-2 (BTKi-2) was located in the lower-right corner (highlighted in green, Fig. 1E), indicating a favorable balance between antiviral activity and cellular tolerance, and demonstrated superior efficacy compared to ST-246 at 5 μM (Fig. 1E). In addition, several BTK-targeting compounds were recurrently identified among the leading hits in the primary screening, suggesting that BTK inhibitors might be potential novel antivirals. Collectively, these results indicate that BTKi-2 is a promising candidate for further development as an antiviral agent against orthopoxvirus infections.

BTKi-2 inhibits MVTT-GFP, ECTV, and MPXV in various cell lines

We initially demonstrated the antiviral activity of BTKi-2 (chemical structure shown in Fig. 2A) at 5 μM during primary screening. To further validate its efficacy, we performed a dose-response assay in which Huh7 cells were infected with MVTT-GFP at a multiplicity of infection (MOI) of 0.02 and treated with increasing concentrations of BTKi-2 or ST-246. Infection rates were quantified via high-content imaging at 24 h p.i. and cytotoxicity was evaluated by measuring intracellular ATP level. Our results indicated that BTKi-2 exhibits a 50% cytotoxicity concentration (CC_{50}) exceeding 20 μM and a 50% inhibitory concentration (IC_{50}) of 0.535 μM, whereas ST-246 displayed an IC_{50} of 0.118 μM (Fig. 2B), underscoring the potent antiviral activity of BTKi-2.

Having established that BTKi-2 inhibits VACV infection in Huh7 cells, we next assessed whether this activity is retained in other cellular backgrounds, and extends to additional orthopoxviruses. MPXV was selected for its public health relevance, whereas ectromelia virus (ECTV) was included as a well-established laboratory orthopoxvirus model. First, to ensure that the antiviral effects of BTKi-2 were not cell-type specific, we conducted a cytopathic effect (CPE) protection assay in both Huh7 and Vero cells. BTKi-2 demonstrated robust antiviral activity in both cell lines (Fig. 2C), confirming that its effects are not attributable to cytotoxicity and that it is effective in diverse cellular conditions. Besides, our data revealed that BTKi-2 effectively reduced the CPE induced by ECTV in Vero cells, with an IC_{50} of 0.397 μM (Fig. 2D). To evaluate BTKi-2's efficacy against MPXV, we employed a GFP-tagged, replication-defective cell culture model named rdMPXV$^{\Delta 96,158}$, which is biologically contained in cell lines expressing these two essential viral proteins to ensure biosafety (Chen et al., 2025) (Fig. 2E). CV-1 cells stably expressing OPG96 and OPG158 (CV-1-96,158) were infected with rdMPXV$^{\Delta 96,158}$ at an MOI of 0.1 and treated with serial concentrations of BTKi-2 or ST-246. At 30 h p.i., infection rates were quantified by high-content imaging. ST-246 demonstrated an IC_{50} of 0.012 μM, consistent with prior reports (Yang et al., 2005), while BTKi-2 exhibited

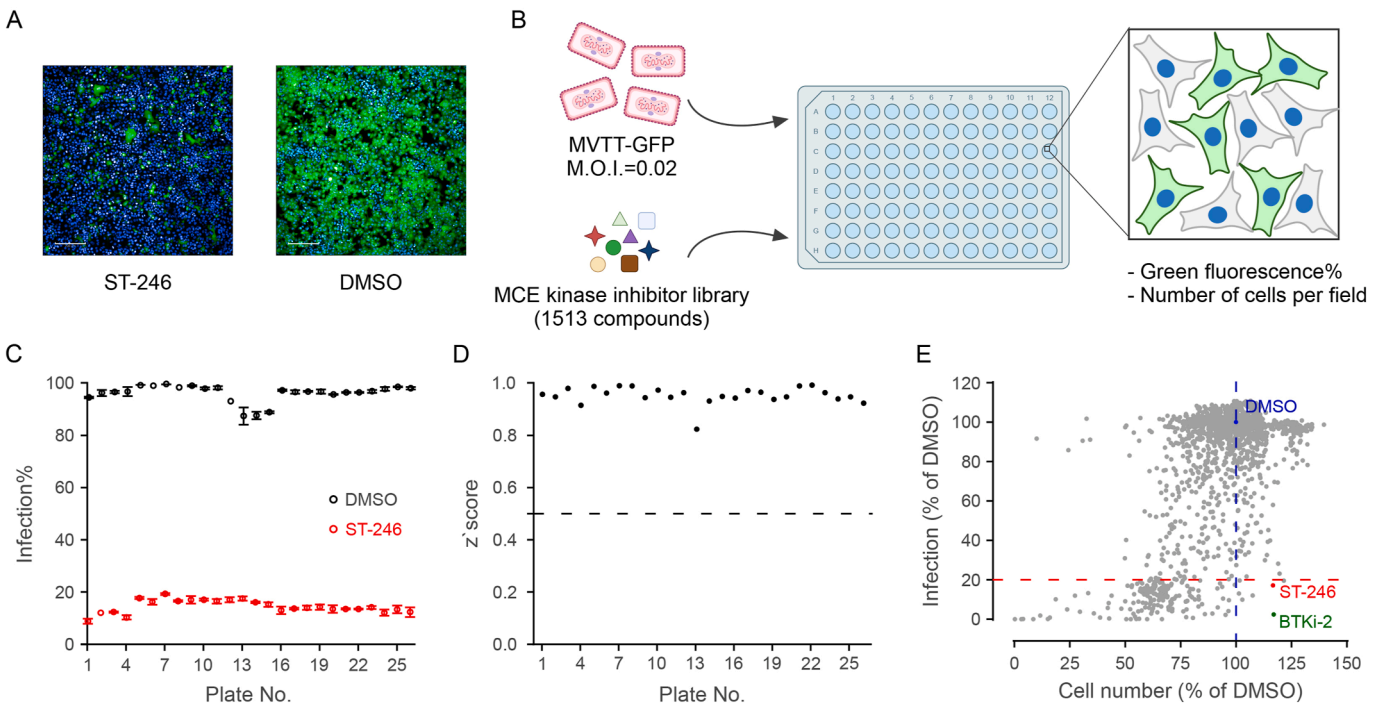

Fig. 1. Identification of BTK inhibitor-2 (BTKi-2) as a potent anti-VACV compound through high-content screening. **A** Representative images from high-content imaging depict MVTT-GFP-infected Huh7 cells treated with 10 μM ST-246 (positive control) or 0.1% (v/v) DMSO (negative control). Green fluorescence indicates infected cells, and blue fluorescence represents nuclei stained with DAPI. Scale bar: 200 μm. **B** Schematic of the high-content screening (HCS) assay workflow: Huh7 cells were infected with MVTT-GFP (MOI = 0.02) and treated with compounds from the MCE kinase inhibitor library (1513 compounds at 5 μM). ST-246 (5 μM) and DMSO (0.05%, v/v) served as positive and negative controls, respectively. After 24 h, cells were fixed, stained with DAPI, and analyzed by HCS to quantify infection rates (GFP%) and cell counts (cytotoxicity). **C** Infection rates of positive (red) and negative (black) control wells treated with ST-246 (red, n = 3 biological replicates) or DMSO (black, n = 3 biological replicates). **D** Z′ factors of the screening plates. Plates with Z′ factors above 0.5 (dashed line) were considered qualified for further analysis. **E** Scatter plot of infection rates (% of DMSO) versus cell numbers (% of DMSO) for all tested compounds. DMSO and ST-246 are marked in blue and red, respectively. BTKi-2 (green) exhibited potent antiviral activity with minimal cytotoxicity.

an IC_{50} of 0.260 μM against MPXV (Fig. 2F). Altogether, these findings demonstrate the antiviral activity of BTKi-2 against multiple orthopoxviruses across different cell lines.

BTKi-2 inhibits poxvirus DNA replication and intermediate/late gene expression

To investigate the stage at which BTKi-2 interferes with poxvirus infection, we performed a time-of-addition assay to distinguish its effects on the pre-entry versus post-entry phases of the viral life cycle (Daelemans et al., 2011; Lin et al., 2024) (Fig. 3A). In Group 1, DMSO, ST-246, or BTKi-2 was added simultaneously with the virus at 37 °C and removed after 1 h; no significant inhibition was observed relative to the DMSO control (Fig. 3B), indicating that BTKi-2 does not affect viral entry. In Group 2, cells were first incubated with virus at 4 °C for 1 h to allow attachment, followed by compound treatment beginning 1 h post-infection to block post-attachment stages. In Group 3, cells were incubated with virus at 37 °C for 1 h to permit virus entry, and compound treatment commenced 1 h post-infection to target post-entry events. In both Groups 2 and 3, BTKi-2 significantly reduced infection rates (Fig. 3B), similar to the inhibition observed with ST-246, a known inhibitor of viral wrapping and release (Duraffour et al., 2015) (Fig. 3C). These results suggest that BTKi-2 acts during the post-entry phase of infection.

Next, we quantified the yield of mature virions (MV) and extracellular enveloped virions (EEV) under BTKi-2 treatment to examine its effects on progeny virion production. Huh7 cells infected with MVTT-GFP were treated with DMSO, 10 μM ST-246, or various concentrations of BTKi-2. After 24 h, both the supernatant and cell-associated virus were harvested and titrated. At an MOI of 0.2, ST-246 markedly reduced the EEV yield to near the limit of detection and decreased the MV yield by approximately 10-fold, whereas BTKi-2 caused a proportional reduction in both MV and EEV yields (Fig. 3D). At an MOI of 2, ST-246, a known inhibitor of EEV production, had little effect on MV yield but reduced EEV by 23%. In contrast, BTKi-2 caused a dose-dependent reduction in both MV and EEV yields (Fig. 3E), suggesting that it disrupts the viral replication cycle prior to the formation of mature virions.

To further define the replication steps affected by BTKi-2, viral early gene mRNA, genomic DNA, and post-replicative gene mRNA levels were evaluated by qPCR, with cytosine arabinoside (AraC) included as a positive control, a nucleoside analog known to interfere with DNA synthesis. Huh7 cells were infected with MVTT-GFP in the presence of DMSO, AraC or BTKi-2. *E3L* mRNA (early gene) was measured at 2 h post-infection, whereas viral genomic DNA, *D13L* mRNA (intermediate gene), and *A3L* mRNA (late gene) were quantified at 8 h post-infection. Neither AraC nor BTKi-2 significantly affected *E3L* mRNA abundance, but both markedly reduced viral DNA levels and *D13L* and *A3L* transcript levels (Fig. 3F). These results indicate that BTKi-2 inhibits viral DNA replication and subsequent intermediate and late gene expression.

BTKi-2 inhibits VACV infection in murine model

To evaluate the therapeutic potential of BTKi-2 *in vivo*, we used a murine model of vaccinia virus (VACV)-induced pneumonia (Zhao et al., 2024). After confirming the tolerability of this dosing regimen in uninfected BALB/c mice (Supplementary Fig. S4), BTKi-2 was administered intraperitoneally (i.p.) at 50 mg/kg, starting 3 h prior to infection and continuing daily from Day 1 to Day 5. The vehicle control was given on the same schedule. Survival, body weight and lung viral loads were monitored throughout the experiment (Fig. 4A).

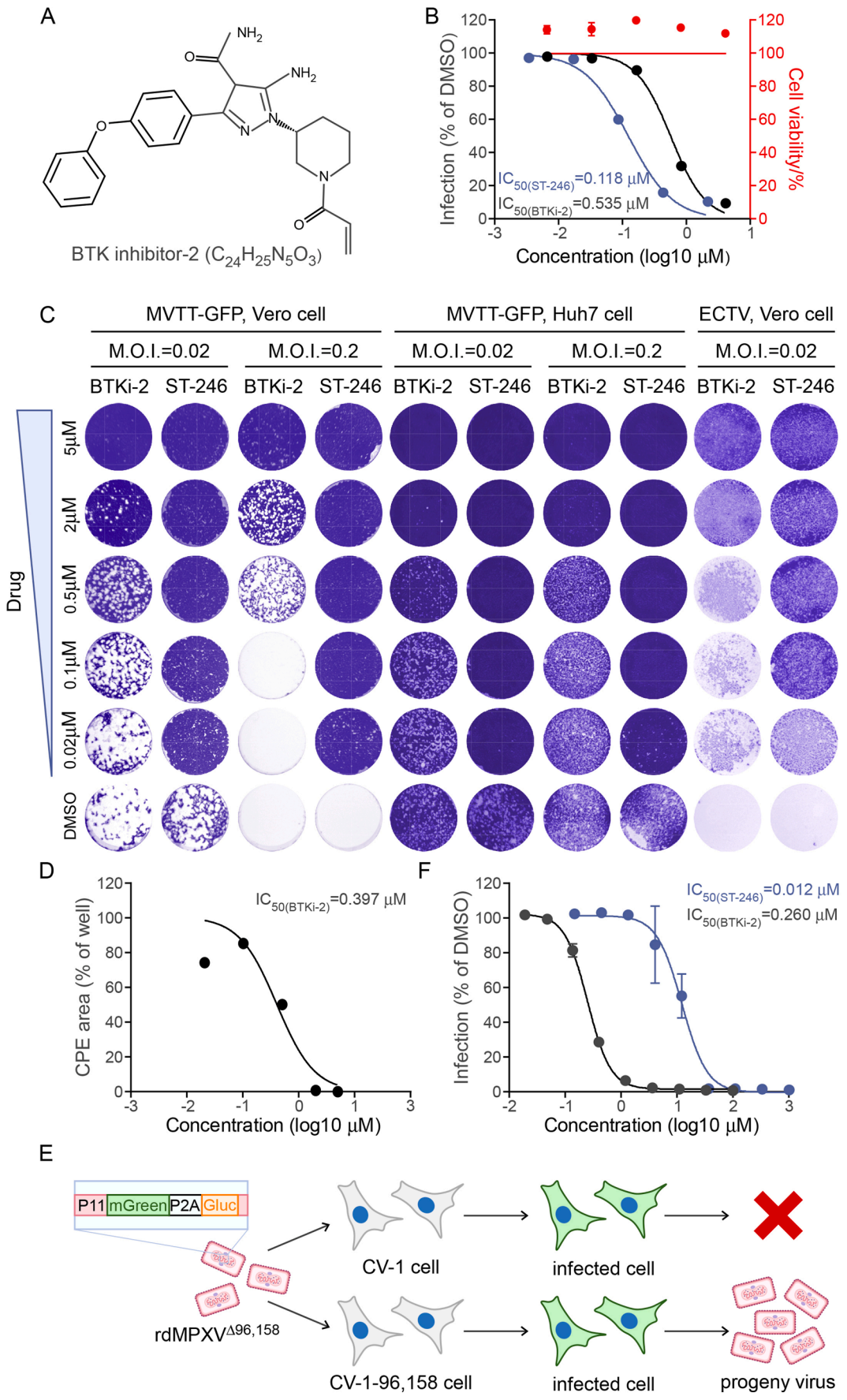

(caption on next page)

Fig. 2. BTKi-2 inhibits MVTT-GFP, ECTV, and MPXV infection *in vitro*. **A** Chemical structure of BTKi-2 ($C_{24}H_{25}N_5O_3$). **B** Dose-response curves for BTKi-2 (black, IC_{50}; red, CC_{50}) and ST-246 (blue). IC_{50} and CC_{50} values were calculated using GraphPad Prism software and represent one of three independent experiments. **C** Cytopathic effect protection assay in Huh7 and Vero cells treated with BTKi-2 or ST-246 at concentrations ranging from 0.02 to 5 μM. Cells were seeded in 24-well plates one day prior to infection with MVTT-GFP or ECTV at MOI = 0.02 or 0.2. At 72 h (Huh7 cells) or 96 h (Vero cells) post-infection, cells were fixed and stained with crystal violet. DMSO (0.05%, v/v) served as the negative control. **D** The IC_{50} value of BTKi-2 against ECTV was calculated using GraphPad Prism software based on CPE areas measured by ImageJ at different drug concentrations. **E** Schematic of the rdMPXV$^{\Delta 96,158}$ cell culture model (Chen et al., 2025). Two genes indispensable for viral assembly, OPG96 and OPG158, were deleted and transcomplemented in CV-1-96,158 cells to ensure biosafety. Besides, the reporter expression cassette, mGreen-Lantern (mGreen)-P2A-Gaussia luciferase, under the control of the viral late promoter P11, was inserted into the thymidine kinase (tk) gene (OPG101) to visualize infection. **F** Dose-response curves for anti-rdMPXV$^{\Delta 96,158}$ activity of BTKi-2 (black) and ST-246 (blue). IC_{50} values were calculated using GraphPad Prism software and represent one of three independent experiments.

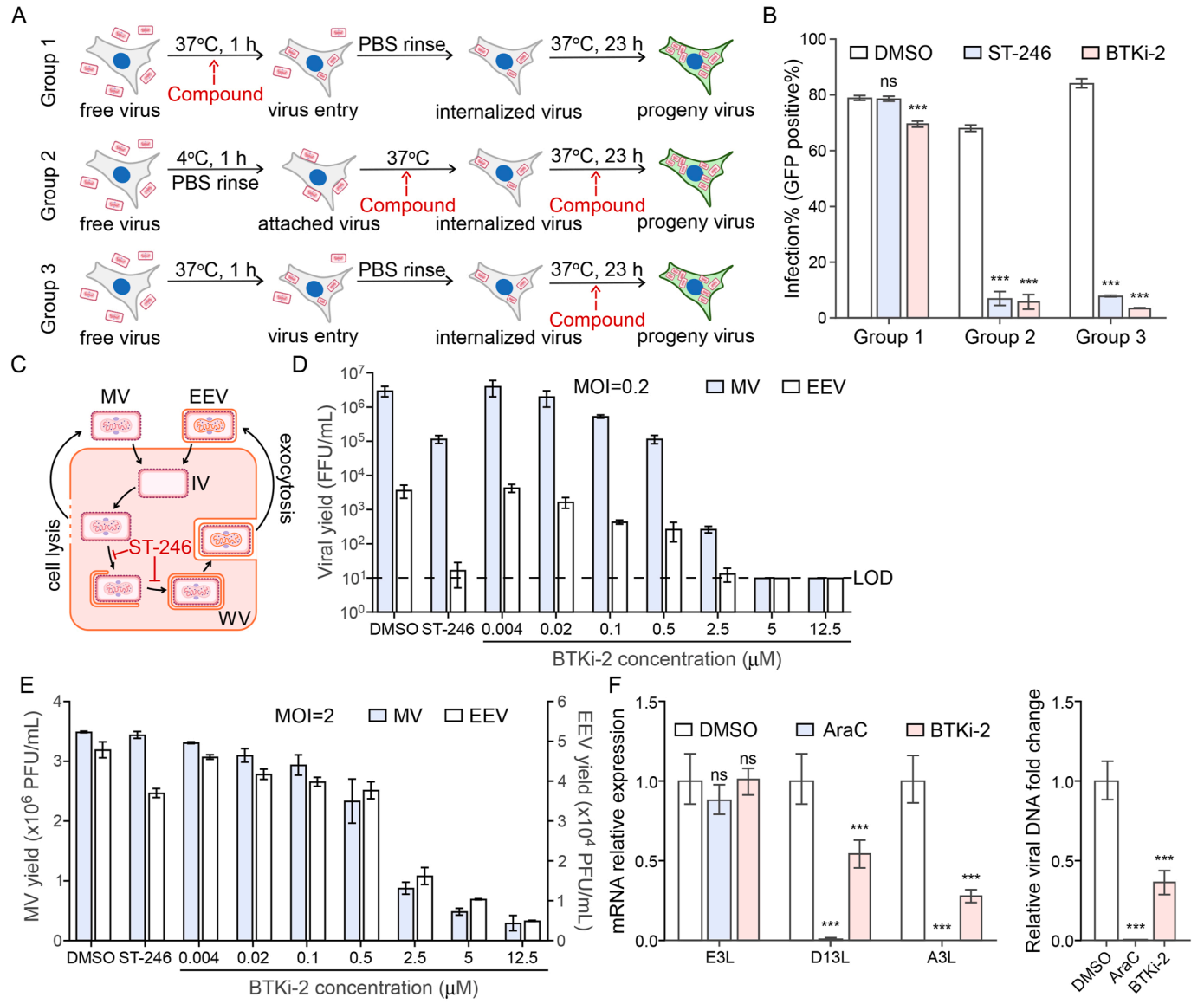

Fig. 3. BTKi-2 disrupts the poxvirus replication cycle. **A** Time-of-addition assay schematic. In Group 1, the drug (DMSO, ST-246, or BTKi-2) was added simultaneously with the virus (MOI = 0.02) at 37 °C for 1 h and then replaced with fresh medium. In Groups 2 and 3, drug treatment commenced 1 h post-infection after virus attachment (4 °C incubation, Group 2) or entry (37 °C incubation, Group 3). Cells were fixed at 24 h p.i. and analyzed by flow cytometry for GFP positivity. **B** Infection rates of MVTT-GFP of each treatment group are shown. ST-246 (blue) served as a positive control, and DMSO (white) as a negative control. Statistical significance was determined by one-way ANOVA with Dunnett's post hoc test; ns, no significance; ***$P < 0.001$. **C** Schematic representation of the VACV life cycle. Following entry, the virus initiates its replication cycle by transcribing and translating its genome to form immature virions (IVs), which mature into intracellular mature virions (MVs). MVs can be released via cell lysis or processed into wrapped virions (WVs) that are exocytosed as extracellular enveloped virions (EEVs). **D** Dose-dependent effects of BTKi-2 and ST-246 on MV and EEV yields at MOI = 0.2. Huh7 cells infected with MVTT-GFP (MOI = 0.2) were treated with DMSO (0.1%, v/v), 10 μM ST-246, or various concentrations of BTKi-2. At 24 h p.i., cell debris (for MVs) and supernatant (for EEVs) were collected and titrated. **E** Dose-dependent effects of BTKi-2 and ST-246 on MV and EEV yields at high MOI. Huh7 cells infected with MVTT-GFP (MOI = 2) were treated with DMSO (0.1%, v/v), 10 μM ST-246, or various concentrations of BTKi-2. At 24 h p.i., cell debris (for MVs) and supernatant (for EEVs) were collected and titrated. **F** Relative quantification of viral gene mRNA and genomic DNA. Huh7 cells infected with MVTT-GFP (MOI = 0.2) were treated with DMSO, AraC (40 μg/mL), or BTKi-2 (10 μM). At 2 h p.i., *E3L* mRNA levels were quantified by RT-qPCR. At 8 h p.i., *D13L* and *A3L* mRNA levels were quantified by RT-qPCR, and viral genomic DNA levels were quantified by qPCR. Gene expression and viral DNA levels were normalized to *GAPDH* for comparison between groups (DMSO = 1). ns, not significant; ***$P < 0.001$.

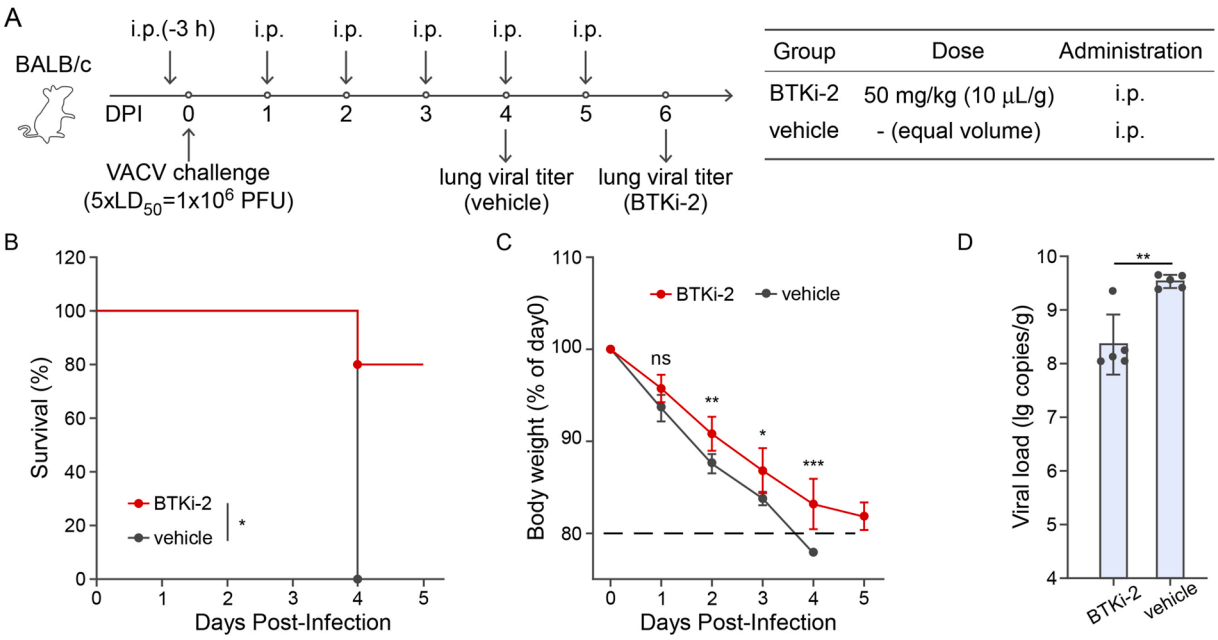

Fig. 4. *In vivo* evaluation of BTKi-2 in a murine model of VACV-induced pneumonia. **A** Experimental design: BALB/c mice (n = 5 per group) received intraperitoneal (i.p.) injections of BTKi-2 (50 mg/kg), or vehicle (matching volume to BTKi-2 group). Three hours later, mice were intranasal (i.n.) challenged with VACV (1×10^6 PFU). From Day 1 to Day 5 post-infection (p.i.), BTKi-2 and vehicle groups received daily i.p. injections. **B** Kaplan-Meier survival analysis over 5 days p.i. for BTKi-2 (red), and vehicle (black) groups. Statistical significance was determined using a Log-rank (Mantel-Cox) test. $^*P < 0.05$. **C** Body weight changes over 5 days p.i., presented as a percentage of initial weight (Day 0) for BTKi-2 (red), and vehicle (black) groups. Statistical significance was assessed by two-way ANOVA followed by Sidak's multiple comparisons test. ns, not significant; $^*P < 0.05$; $^{**}P < 0.01$; $^{***}P < 0.001$. **D** Viral loads in lung were measured by quantitative real-time PCR (qPCR). Statistical significance was assessed by unpaired, two-tailed *t*-test. $^{**}P < 0.01$.

All vehicle-treated mice died by Day 4. In contrast, only one animal in the BTKi-2 group died by Day 4, yielding a significantly improved survival curve compared to vehicle-treated animals (Fig. 4B). Consistent with these findings, vehicle-treated mice exhibited a precipitous weight loss preceding death, whereas BTKi-2-treated mice lost weight more slowly (Fig. 4C). Furthermore, quantitative PCR of lung homogenates at the terminal time point demonstrated a significant viral load reduction of ~90% in the BTKi-2 group compared with vehicle-treated animals (Fig. 4D). Collectively, these data indicate that BTKi-2 markedly suppresses VACV replication in lungs and modestly prolongs survival, supporting further mechanistic exploration and optimization before clinical application.

BTKi-2 exerts antiviral activity beyond EGFR, ERBB2, and BTK

To elucidate the molecular target underlying the antiviral effects of BTKi-2, we first considered Bruton's tyrosine kinase (BTK), which is essential for B-cell maturation and activation (Fluckiger et al., 1998). However, given that BTK expression is largely restricted to B cells and myeloid cells (Jefferies et al., 2003), it is unlikely to account for the antiviral effect observed in Huh7 cells. Supporting this view, analysis of our screening results showed that among the 36 BTK inhibitors included in the library, only 7 were able to reduce VACV infection to below 50% (Supplementary Table S1; Supplementary Fig. S2). Additionally, two clinically used BTK inhibitors, pirtobrutinib and zanubrutinib, exhibited only modest antiviral activity in Huh7 cells (Supplementary Fig. S3). This trend suggests that the antiviral activity of BTKi-2 is likely mediated by mechanisms independent of BTK inhibition. Previous studies have reported that BTK inhibitors can also suppress other non-receptor tyrosine kinases, such as BMX, Itk, Tec, Txk, EGFR, Blk, ErbB2, ErbB4, and JAK3, when used at higher doses (Estupiñán et al., 2021; Shaw, 2020; Tasso et al., 2021). To determine which of these potential targets might contribute to the antiviral effects of BTKi-2, we performed RT-qPCR in Huh7 cells to measure the expression of these kinases. Our data showed that EGFR and ERBB2 were expressed at appreciable levels, whereas mRNA levels of the other kinases were negligible (Fig. 5A). Based on previous reports implicating EGFR in VACV infection (Beerli et al., 2019), where inhibitors like gefitinib block viral spread by suppressing the ERK1/2 pathway (Langhammer et al., 2011), the inhibition of EGFR and/or ERBB2 was considered a plausible mechanism.

To test this hypothesis, we generated Huh7 cell lines with single or double knockouts (KOs) of EGFR and ERBB2 and assessed their impact on VACV infection. In plaque formation assays, both EGFR and ERBB2 KOs led to significantly reduced plaque sizes (Fig. 5B–C), consistent with their roles in viral dissemination (Beerli et al., 2019; Buller et al., 1988). However, neither the overall infection rate of MVTT-GFP (Fig. 5D) nor the yield of progeny virus (Fig. 5E) was significantly affected in these KO cell lines. These findings indicate that, although EGFR and ERBB2 influence viral transmission, their inhibition alone cannot fully account for the antiviral activity of BTKi-2.

To further assess the contribution of BTK to VACV infection and to the antiviral activity of BTKi-2, we performed BTK knockdown in BTK-expressing HEK293T (Fig. 5F) and HeLa cells (Fig. 5H). The reduction of BTK was demonstrated by Western blotting analysis. To determine whether BTK knockdown affects the antiviral activity of BTKi-2, HEK293T cells were transfected with siNC or BTK-targeting siRNAs 1# – 3# for 48 h and then infected with MVTT-GFP at an MOI of 0.2 in the presence of 2 μM BTKi-2 or 0.02% DMSO (v/v). At 24 h p.i., cells were lysed and progeny MV was harvested for titration (Fig. 5G). Two-way ANOVA revealed that BTKi-2 treatment accounted for 98.92% of total variation ($P < 0.0001$), and that neither BTK knockdown alone ($P = 0.1536$) nor the interaction between BTK knockdown and BTKi-2 treatment ($P = 0.5170$) was statistically significant. Similar results were observed in HeLa cells (Fig. 5I), in which BTKi-2 treatment accounted for 98.13% of total variation ($P < 0.0001$) and the effect of BTK knockdown and their interaction were not significant ($P = 0.1402$,

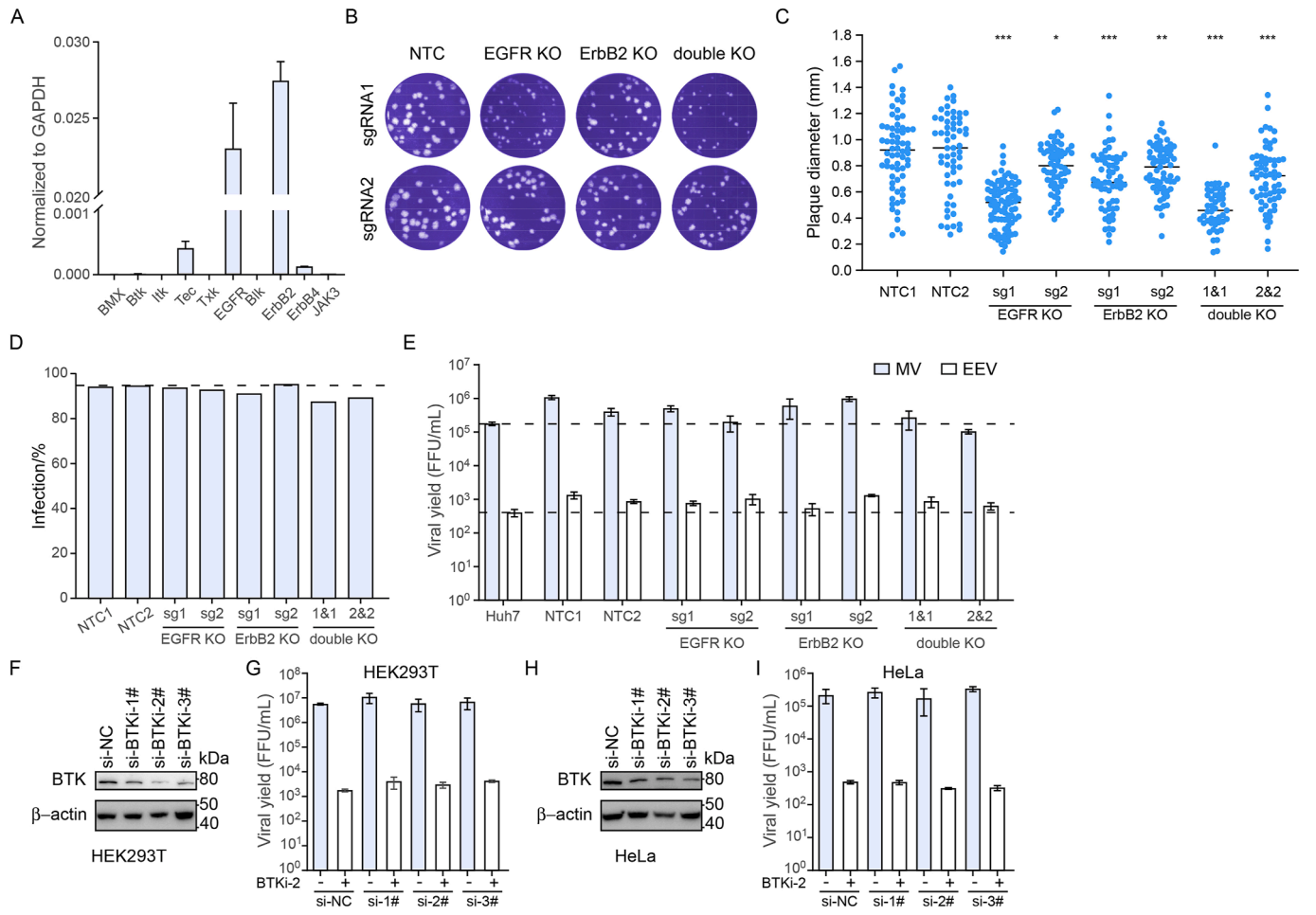

Fig. 5. The antiviral activity of BTKi-2 cannot be fully explained by BTK, EGFR, or ERBB2. **A** Total RNA from Huh7 cells was extracted, reverse transcribed, and the mRNA levels of the indicated kinases were quantified by RT-qPCR. Values were normalized to GAPDH mRNA levels. **B** Cells (2×10^5 per well in 24-well plates) were infected with 80 FFU of MVTT-GFP per well. After 72 h, cells were fixed with 4% paraformaldehyde (PFA), washed with PBS, and stained with crystal violet. "sgRNA1" and "sgRNA2" indicate different single-guide RNAs (sgRNAs) used for CRISPR/Cas9-mediated gene knockout. **C** Quantification of plaque diameters from (**B**). Each dot represents a single plaque, with the horizontal line indicating the mean plaque diameter. Statistical significance was assessed by one-way ANOVA followed by Dunnett's multiple comparisons test. $^*P < 0.05$; $^{**}P < 0.01$; $^{***}P < 0.001$. **D** Cells with genes knockout as indicated were infected at an MOI of 0.02 and fixed for flow cytometry at 24 h post-infection (p.i.). **E** Viral yields (MV and EEV) in naïve, NTC, EGFR KO, ERBB2 KO, and double KO cell lines. Cells were infected with MVTT-GFP at an MOI of 0.2. At 24 h p.i., supernatants (for EEV) and cell debris (for MV) were collected and titrated. Data represent mean ± SD from three independent experiments. **F** Validation of BTK knockdown in HEK293T cells. HEK293T cells were transfected with 80 nM BTK-targeting siRNAs (siRNA-1, siRNA-2, and siRNA-3) or a negative control siRNA (siNC). At 48 h post-transfection, cells were harvested and lysed in 1 × SDS loading buffer, followed by Western blot analysis using anti-BTK and anti-β-actin antibodies. **G** Viral yields in BTK-knockdown HEK293T cells. HEK293T cells were transfected with 80 nM BTK-targeting siRNAs (siRNA-1, siRNA-2, and siRNA-3) or siNC for 48 h and then infected with MVTT-GFP at an MOI of 0.2 in the presence or absence of 2 μM BTKi-2. At 24 h p.i., cell debris were collected and titrated. Data represent mean ± SD from three independent experiments. Statistical significance was assessed by two-way ANOVA followed by Sidak's multiple comparisons test. **H** Validation of BTK knockdown in HeLa cells. HeLa cells were transfected with 80 nM BTK-targeting siRNAs (siRNA-1, siRNA-2, and siRNA-3) or a negative control siRNA (siNC). At 48 h post-transfection, cells were harvested and lysed in 1 × SDS loading buffer, followed by Western blot analysis using anti-BTK and anti-β-actin antibodies. **I** Viral yields in BTK-knockdown HeLa cells. HeLa cells were transfected with 80 nM BTK-targeting siRNAs (siRNA-1, siRNA-2, and siRNA-3) or siNC for 48 h and then infected with MVTT-GFP at an MOI of 0.2 in the presence or absence of 2 μM BTKi-2. At 24 h p.i., cell debris were collected and titrated. Data represent mean ± SD from three independent experiments. Statistical significance was assessed by two-way ANOVA followed by Sidak's multiple comparisons test.

$P = 0.2430$, respectively). These results indicate that the antiviral activity of BTKi-2 cannot be fully explained by BTK inhibition alone. Further studies are needed to identify the precise mechanism of action.

DISCUSSION

Using a high-content screening platform based on the MVTT-GFP cell culture model, we identified BTKi-2 as a promising anti-VACV candidate (Fig. 1). Subsequent dose-response and cytopathic effect protection assays confirmed its efficacy in both Huh7 and Vero cells, with minimal cytotoxicity and an IC_{50} of 0.535 μM (Fig. 2A–C). Moreover, BTKi-2 exhibited potent anti-ECTV activity in Vero cells (IC_{50} = 0.397 μM) (Fig. 2C), anti-MPXV activity in the rdMPXV$^{\Delta 96,158}$ system (IC_{50} = 0.260 μM) (Fig. 2D–E) and significantly reduced lung viral loads by approximately 90% in a murine model of VACV-induced pneumonia, resulting in improved survival compared to vehicle-treated controls (Fig. 4). These findings suggest that BTKi-2 holds potential for mitigating poxvirus infections.

To investigate the mechanism of action, we first performed time-of-addition assays, which revealed that BTKi-2 exerts its antiviral effect after viral entry. Progeny virus inhibition assays further demonstrated that viral yield is suppressed prior to the formation of mature virions, and the quantification of viral early gene mRNA, genomic DNA, and intermediate/late gene mRNAs further implied that BTKi-2 disrupts

viral DNA replication and post-replicative gene expression (Fig. 3). This pattern is consistent with previous findings for another BTK inhibitor, ibrutinib, which was also shown to suppress VACV-WR DNA replication and post-replicative gene expression. Given that BTKi-2 and ST-246 target distinct stages of viral life cycle, the combination therapy may produce additive or synergistic inhibition and mitigate the emergence of drug resistance.

To elucidate the host targets of BTKi-2, we assessed the expression of reported targets of BTK inhibitors in Huh7 cells. Surprisingly, among several candidates, only EGFR and ERBB2 were appreciably expressed (Fig. 5A). Although knockout of EGFR and ERBB2 led to smaller plaques, it did not significantly alter the overall infection rate or progeny virus production (Fig. 5B–E). These findings are not necessarily inconsistent, because plaque size reflects the efficiency of cell-to-cell spread, which depends not only on progeny virus production but also on additional processes such as the formation of cell-associated enveloped virions, actin tail formation, and cell motility. Consistent with our results, previous studies showed that inhibition of the EGFR pathway reduced VACV-WR plaque size mainly by interfering with actin tail formation, rather than substantially affecting MV or EEV production (Beerli et al., 2019). We further assessed the contribution of BTK to the antiviral activity of BTKi-2 in cells with endogenous BTK expression. In HEK293T and HeLa cells, the antiviral activity of BTKi-2 was retained after BTK knockdown (Fig. 5G and I). These findings demonstrate that the antiviral activity of BTKi-2 might not be attributed to any single target such as EGFR, ERBB2 or BTK. Besides, we noticed that although BTK was reported as a proviral factor (Niu et al., 2025), BTK knockdown did not impair progeny virus yield in our assay. One possible explanation is that the contribution of BTK may be context-dependent and influenced by differences in virus strain, infection conditions, assay endpoint, or the extent of BTK knockdown. Maybe a stronger proviral contribution of BTK could be observed under low-MOI and longer-duration conditions.

In addition to BTKi-2, our top candidate, we observed a recurrent presence of compounds annotated as BTK or EGFR inhibitors among the active hits in our library. Among the eight primary hits with a selective index > 2 during validation, we noticed an enrichment for inhibitors nominally targeting BTK and EGFR: three of them (BTKi-2, ibrutinib, and ONO-4059 analog) are classified as BTK inhibitors, whereas three of them (TAS6417, genistein, and lifirafenib) are annotated as EGFR inhibitors (Supplementary Fig. S1). A similar trend was previously reported in a drug-repurposing screen for anti-poxvirus compounds, in which 142 hits were identified from 3228 candidates, including two BTK inhibitors (ibrutinib and CNX-774) and twenty-three VEGFR/EGFR inhibitors (Peng et al., 2020). However, only a small fraction of BTK- or EGFR-targeting compounds in the library exhibited meaningful antiviral activity (Supplementary Table S1; Supplementary Fig. S2). These observations support that their antiviral activity results from additional cellular mechanisms beyond BTK or EGFR inhibition. A systematic comparison of the target spectra of the most potent antiviral hits may therefore help identify previously unrecognized host factors that are genuinely required for orthopoxvirus replication.

Nonetheless, our study has limitations. First, our screening approach focused on a library of known kinase inhibitors, possibly overlooking critical host factors that are not common drug targets. Thus, an unbiased whole kinase screening based on genetic tools might be helpful. However, CRISPR/Cas9 whole-genome screens have not identified any single kinase as indispensable for poxvirus infection (Matía et al., 2022), suggesting that the potent antiviral effect of BTKi-2 may stem from its ability to modulate a complex network of host factors.

Furthermore, although BTKi-2 effectively reduces mortality and viral load *in vivo*, a deeper understanding of its interplay with host immune networks should be prioritized before clinical translation. BTK is indispensable for B cell development and influences macrophage function (Lee et al., 2012). It has been reported that B-cell-deficient mice had a normal early T-cell response to ECTV yet ultimately died of persistent high virus load in the blood, lungs, and skin (Chaudhri et al., 2006). Similar results have been obtained in macaques, where anti-vaccinia antibodies alone were sufficient to prevent deadly MPXV infection (Edghill-Smith et al., 2005). These observations underscore the need to delineate how BTKi-2 affects B-cell function and antibody production during orthopoxvirus infection, and to identify a therapeutic window that preserves protective humoral immunity while maintaining optimal antiviral efficacy.

In addition, tissue damage during viral infection may not result solely from direct viral replication, but may also be driven by dysregulated host inflammatory responses. In immunocompromised patients with severe or fatal infection, MPXV-associated immune reconstitution inflammatory syndrome (IRIS) may contribute to disease progression (Ritter et al., 2024). Beyond its role in B cells, BTK also participates in innate immune signaling in myeloid cells and promotes the production of pro-inflammatory mediators. Ibrutinib has been reported to possibly protect against pulmonary injury and decrease blood inflammatory cytokines in Waldenstrom macroglobulinemia (WM) patients infected with SARS-CoV-2 (Treon et al., 2020). Acalabrutinib, another BTK inhibitor, was reported to reduce inflammation and improve clinical outcome of nineteen hospitalized patients with severe COVID-19 (Roschewski et al., 2020). In the context of orthopoxvirus infection, it will therefore be important to determine whether BTKi-2 influences not only viral replication but also the host inflammatory response, as both may contribute to its overall *in vivo* effect.

CONCLUSIONS

In summary, our findings provide compelling evidence that BTKi-2 is an effective antiviral agent against VACV *in vivo* and *in vitro*, with similar efficacy against ECTV and MPXV in cell culture. Mechanistically, BTKi-2 suppresses viral DNA replication and intermediate/late gene expression. However, its antiviral activity cannot be fully explained by inhibition of BTK, EGFR, or ERBB2 alone. Further identification of its molecular target(s) will not only facilitate the optimization of BTKi-2, but also improve our understanding of orthopoxvirus-host interactions and support the development of antiviral strategies against orthopoxvirus infections.

MATERIALS AND METHODS

Cell culture

All cell lines used in this study were obtained from the American Type Culture Collection (ATCC, Manassas, VA, USA). Huh7, Vero, HEK293T, and HeLa cells were maintained in Dulbecco's Modified Eagle Medium (DMEM) supplemented with 10% fetal bovine serum (FBS) and 50 IU/mL penicillin/streptomycin (P/S) in a humidified 5% CO_2 incubator at 37 °C. Cells were passaged every 2–3 days and harvested at 90%–95% confluence for experiments. All cell lines were tested regularly to ensure the absence of mycoplasma contamination using PCR-based assays (Young et al., 2010).

Virus amplification and titration

GFP reporter gene was inserted into the genome of modified Tiantan strain of vaccinia virus (MVTT-GFP) to visualize viral infection (Zhu et al., 2007). For amplification, Huh7 cells in 10-cm dishes were infected at an MOI of 0.01 and incubated for 48 h until extensive cell detachment was observed. Cells and supernatant were collected and centrifuged at $500\times g$ for 5 min. The cell pellet was resuspended in 1 mL PBS and subjected to six freeze-thaw cycles (freezing in liquid nitrogen for 1 min followed by thawing in a 37 °C water bath for 2–3 min) to release intracellular mature virus (MV). The resulting supernatant, containing both MV and extracellular enveloped virus (EEV), was pooled, aliquoted, and stored at −80 °C. For titration, Huh7 cells seeded in 96-well

plates (2×10^4 cells/well) were infected with 100 μL of serial 10-fold dilutions (10^{-1} to 10^{-8}) in DMEM (containing 10% FBS, 50 IU/mL P/S), in triplicate. Foci were counted 36–48 h post infection, yielding a typical titer of 1×10^6 focus forming units (FFU)/mL.

Ectromelia virus (ECTV) was amplified and titrated in Vero cells. For amplification, Vero cells seeded in 10-cm dishes were infected at an MOI of 0.01 and cultured in DMEM without FBS but supplemented with 50 IU/mL P/S. After 4–5 days, similar protocol was used to harvest and store MV and EEV. For titration, Vero cells were seeded into 96-well plates at 1×10^4 cells per well one day prior to titration. On the following day, cells were infected with 100 μL of serially diluted virus (10^{-0} to 10^{-7}) in DMEM (without FBS, 50 IU/mL P/S), with each dilution performed in triplicate. Plaques were counted 60–72 h post-infection, yielding a typical titer of 2×10^5 plaque forming units (PFU)/mL.

Chemicals and reagents

The MedChemExpress Kinase Inhibitor Library, containing 1513 kinase inhibitors, was customized and housed at the Center of Pharmaceutical Technology, Tsinghua University (Beijing, China), was utilized for HCS and dose-response studies. The collection was provided in 384-well plates, with each compound dissolved to 10 mM and stored at −20 °C until use. ST-246 was acquired from SelleckChem (S3380). BTK inhibitor 2 was purchased from TargetMol (T10629). DMSO was purchased from Sigma (D2650-100 ML).

High-content screening for antiviral compounds

One day prior to infection, Huh7 cells were seeded in clear 96-well plates (167,008, ThermoFisher Scientific) at a density of 20,000 cells per well. The 10 mM drug stocks were thawed at 25 °C for 1 h before use. Using the Echo550 Liquid Handler (Labcyte), 50 nL of each compound was transferred into empty 96-well round-bottom plates (163,320, ThermoFisher Scientific). Positive control (10 mM ST-246 in DMSO) and negative control (DMSO) were processed similarly. Next, 100 μL of an MVTT-GFP dilution in DMEM (supplemented with 10% FBS and 50 IU/mL P/S) was added to achieve a final drug concentration of 5 μM (0.05% DMSO, v/v) and an MOI of 0.02. The resulting drug-virus mixture replaced the culture medium of Huh7 cells. At 24 h post-infection, cells were fixed with 4% PFA (Leagene) at room temperature for 15 min and stained with 1 μg/mL DAPI (in PBS) for 2 h. Samples were then analyzed using the Opera Phenix High-Content Screening System (PerkinElmer) and Harmony software (PerkinElmer) to quantify total and GFP-positive cell numbers across five fields per well. Plate quality was assessed by Z′ factor using the formula: Z' = 1 − 3*(SD of positive control + SD of negative control)/|mean of positive control − mean of negative control| (Zhang et al., 1999). Finally, each compound's infection rate and cell count were normalized to those of the negative control on the same plate for further summarization and analysis.

Dose-response curves determination

For IC_{50} determination, Huh7 cells were seeded at 20,000 cells per well in 96-well plates and infected with MVTT-GFP at an MOI of 0.02. Compounds were added at a series of gradient concentrations. At 24 h p.i., cells were fixed, stained with DAPI, and analyzed using the Opera Phenix high-content screening system to quantify GFP-positive cells as previously described. The infection rate in each well was normalized to that of the DMSO control, and IC_{50} values were calculated by fitting the data to the "log (inhibitor) vs. normalized response-variable slope" model using GraphPad Prism 8.4.3 (GraphPad Software).

For CC_{50} determination, Huh7 cells were seeded at 5000 cells per well in 96-well plates and cultured overnight. The following day, cells were treated with serial dilutions of each compound. After 3 days, cell viability was assessed using the CellTiter-Glo® Reagent Kit (G7571, Promega) according to the manufacturer's instructions. Luminescence was measured in opaque-walled 96-well plates using a Promega luminometer, and CC_{50} values were determined by fitting the data to the "log (inhibitor) vs. normalized response-variable slope" model in GraphPad Prism 8.4.3, with DMSO-only samples serving as the 100% viability control.

Cytopathic effect protection assay

Huh7 or Vero cells were seeded in 24-well plates at 150,000 cells per well one day before infection. Cells were then infected with MVTT-GFP or ECTV at an MOI of 0.02 in the presence of varying doses of the test compound or DMSO as a control. For MVTT-GFP, cells were cultured in DMEM supplemented with 10% FBS and 50 IU/mL penicillin/streptomycin, whereas for ECTV, DMEM without FBS (with 50 IU/mL P/S) was used. At 72 h p.i. (MVTT-GFP) or 96 h p.i. (ECTV), cells were fixed with 4% PFA and stained with 1% (w/v) crystal violet in PBS. Photographs of each well were captured by Multifunctional Imaging System (Tanon 1600). Plaque areas formed by ECTV under different drug concentrations were quantified using ImageJ software. The inhibition% was calculated as [1 − (plaque area/well area)] × 100%, and was imported into GraphPad Prism for dose–response curve fitting and IC_{50} determination.

rdMPXV$^{\Delta 96,\ 158}$ inhibition assay

Replication defective MPXV lacking OPG96 and OPG158 (rdMPXV$^{\Delta 96,\ 158}$) was used to evaluate the antiviral activity of compounds as reported (Chen et al., 2025). Briefly, CV-1-96, 158 cells, which had been engineered to transcomplement the essential viral proteins for assembly, were seeded into 96-well plates and infected with rdMPXV$^{\Delta 96,158}$ at an MOI of 0.1 in the presence of serial compound dilutions. After 30 h of incubation, cells were fixed, stained with DAPI, and analyzed as detailed in the "Dose-Response Curves Determination" section.

Viral yield inhibition assay

Huh7 cells were seeded in 24-well plates at 2×10^5 cells per well and cultured overnight. The following day, cells were incubated with MVTT-GFP (MOI = 0.2 or 2) at 37 °C for 1 h to allow for viral entry. After 1 h, the supernatant was discarded, and the cells were rinsed twice with PBS to remove remaining virus. Subsequently, 500 μL of DMEM (containing 10% FBS and 50 IU/mL P/S), containing either the test compound or DMSO, was added to each well. At 24 h p.i., progeny EEV and MV were harvested and titrated.

VACV infection assay in BALB/c mice

Experiments were performed in the Animal Biosafety Level 2 (ABSL-2) facility at the Chinese Center for Disease Control and Prevention (Zhao et al., 2024). Specific pathogen-free, 6-8-week-old female BALB/c mice were purchased from Beijing Vital River Laboratory Animal Technology (licensed by Charles River) and were randomly housed with five mice per cage. BTKi-2 was formulated at 5 mg/mL in vehicle containing 10% DMSO, 40% PEG-300, 5% Tween-80, and 45% saline (v/v). Two groups of mice were intraperitoneally (i.p.) administered BTKi-2 or the vehicle at 10 μL/g body weight (corresponding to a BTKi-2 dose of 50 mg/kg) 3 h prior to intranasal (i.n.) challenge with a lethal dose (1×10^6 PFU) of VACV-WR. Over the following 4−5 days, BTKi-2 or the vehicle was administered once daily at the same volume. Mice were weighed daily and were euthanized when they lost 20% of their initial body weight. Lung tissues were harvested for DNA isolation using the Magnetic Swab Viral DNA/RNA Kit (EnerTher). Viral load was assessed using the NovoStart® Probe qPCR SuperMix (UDG) Kit (Novoprotein) and Premix Ex Taq™(Probe qPCR) (Takara) on the ABI QuantStudio 3 Real-Time PCR system.

RNA isolation and RT-qPCR

The protocol of total RNA extraction, reverse transcription and quantitative PCR analysis has been previously described (Zhu et al., 2024). Primers used in qPCR are shown in Supplementary Table S2.

Generation of EGFR and ERBB2 knockout Huh7 cell lines

LentiCRISPRv2 vector was used to generate EGFR and ERBB2 knockout (KO) Huh7 cell lines (Sanjana et al., 2014). Two target sequences were picked for each gene, and non-target controls (NTCs) with sequence absent from human genome were included as mock KO controls. The targets sequences are shown in Supplementary Table S3. The constructed vectors were verified by Sanger sequencing (Tsingke, Beijing) and used for lentivirus packaging as following the standard protocol (Ren et al., 2021). Huh7 cells were transduced with the lentiviruses twice in the presence of polybrene (10 μg/mL) and subsequently selected by puromycin (5 μg/mL) or blasticidin S (5 μg/mL) treatment to enrich for successfully transduced cells.

Plaque forming assay

Huh7 cells were seeded in 24-well plates at 150,000 cells per well. The next day, cells were infected with 50 focus forming units (FFU) of MVTT-GFP per well. After 1 h of incubation at 37 °C, 250 μL of carboxymethyl cellulose (CMC) overlay was slowly added to each well. At 72 h p.i., cells were fixed with 4% PFA and stained with 1% (w/v) crystal violet in PBS. Photographs of each well were captured by Multifunctional Imaging System (Tanon 1600) and the area and diameter of each plaque were measured using ImageJ Software.

BTK knockdown and Western blotting analysis

HEK293T and HeLa cells were transfected with BTK-siRNA NC or siRNA 1–3 (shown in Supplementary Table S2, ordered from GENCEFE Biotech, Wuxi, China) for 48 h and were infected with MVTT-GFP at MOI of 0.2 in the presence or absence of 2 μM BTKi-2. At 24 h p.i., cells were lysed in 1 × SDS loading buffer. Western blotting was performed as previouisly described (Yang et al., 2024). The membranes were incubated with primary antibodies mouse anti-β-actin (AC004, Abclonal) and rabbit anti-BTK (CSB-PA002867LA01HU, CUSABIO) in 5% nonfat milk in PBS containing 0.1% Tween-20 (PBS-T) for 2 h, followed by washing with PBS-T. The membranes were then incubated with HRP-conjugated secondary antibodies (Abclonal) for 1 h, washed again with PBS-T, and visualized using an ImageQuant LAS 4000 luminescent image analyzer (GE Healthcare).

Statistical analysis

Unless otherwise mentioned, results are represented as means ± standard deviations (SD) determined by GraphPad Prism 8 (GraphPad Software, La Jolla, CA). Dose-response curves were analyzed and fitted with the model 'log (inhibitor) vs. normalized response-variable slope' in GraphPad Prism 8. One-way analysis of variance (ANOVA) with Dunnett's honestly significant difference (HSD) test was used to test for the statistical significance of the differences between the control group and other groups. *P* values of less than 0.05 were considered statistically significant.

DATA AVAILABILITY

All data generated or analyzed during this study are included in this published article (and its supplemental files).

ETHICS STATEMENT

All animal experiments were conducted in compliance with the guidelines and regulations of animal welfare and were approved by the Animal Ethics Committee (approval No. APIMCAS2022124).

AUTHOR CONTRIBUTIONS

Chen Yang: conceptualization, data curation, formal analysis, investigation, methodology, project administration, validation, visualization, writing-original draft, writing-review & editing; Runchu Zhao: formal analysis, investigation, methodology, visualization, writing-original draft; Shuting Huo: investigation; Yaqing Zhang: investigation; Jingxi Feng: investigation; Mingli Gong: investigation; Lin Zhu: investigation; Conggang Zhang: methodology, resources; Linqi Zhang: methodology, resources; Jing Xue: methodology, resources, supervision; Rong Zhang: investigation, methodology, resources, supervision; Qihui Wang: methodology, resources, supervision; Qiang Ding: conceptualization, data curation, formal analysis, funding acquisition, investigation, methodology, project administration, resources, supervision, validation, visualization, writing-original draft, writing-review & editing.

CONFLICT OF INTEREST

The authors declare no competing interests. Prof. Qiang Ding is editorial board member for *Virologica Sinica* and was not involved in the editorial review or the decision to publish this article.

ACKNOWLEDGEMENTS

We thank Center of Pharmaceutical Technology, Tsinghua University for technical supports. This work was supported by National Natural Science Foundation of China (82241077) and Tsinghua University Dushi Program. The funders had no role in study design, data collection and analysis, publication decisions, or manuscript preparation.

APPENDIX A. SUPPLEMENTARY DATA

Supplementary data to this article can be found online at https://doi.org/10.1016/j.virs.2026.06.011.

REFERENCES

Adler, H., Gould, S., Hine, P., Snell, L.B., Wong, W., Houlihan, C.F., Osborne, J.C., Rampling, T., Beadsworth, M.B., Duncan, C.J., Dunning, J., Fletcher, T.E., Hunter, E. R., Jacobs, M., Khoo, S.H., Newsholme, W., Porter, D., Porter, R.J., Ratcliffe, L., Schmid, M.L., Semple, M.G., Tunbridge, A.J., Wingfield, T., Price, N.M., NHS England High Consequence Infectious Diseases (Airborne) Network, 2022. Clinical features and management of human monkeypox: a retrospective observational study in the UK. Lancet Infect. Dis. 22, 1153–1162.

Beerli, C., Yakimovich, A., Kilcher, S., Reynoso, G.V., Fläschner, G., Müller, D.J., Hickman, H.D., Mercer, J., 2019. Vaccinia virus hijacks EGFR signalling to enhance virus spread through rapid and directed infected cell motility. Nat. Microbiol. 4, 216–225.

Buller, R.M.L., Buller, R.M., Chakrabarti, S., Moss, B., Fredrickson, T.N., Fredricksont, T., 1988. Cell proliferative response to vaccinia virus is mediated by VGF. Virology 164, 182–192.

Chaudhri, G., Panchanathan, V., Bluethmann, H., Karupiah, G., 2006. Obligatory requirement for antibody in recovery from a primary poxvirus infection. J. Virol. 80, 6339–6344.

Chen, J., Hu, L., Vernuccio, R., Shi, N., Tian, J., Zhang, Y., Tian, S., Cao, X., Ha, Z., Lu, J., Battini, L., Raynal, B., Haouz, A., Xue, J., Cai, Q., Zhao, Y., Lu, Y., Smith, G.L., Xie, Y., Lu, H., Guardado-Calvo, P., Zhang, P., Zhang, R., 2025. Development of a replication-defective mpox virus platform for fundamental and therapeutic research. Nat. Commun. 17, 798.

Daelemans, D., Pauwels, R., De Clercq, E., Pannecouque, C., 2011. A time-of–drug addition approach to target identification of antiviral compounds. Nat. Protoc. 6, 925–933.

De Clercq, E., Jiang, Y., Li, G., 2023. Therapeutic strategies for human poxvirus infections: Monkeypox (mpox), smallpox, molluscipox, and orf. Trav. Med. Infect. Dis. 52, 102528.

Duraffour, S., Lorenzo, M.M., Zöller, G., Topalis, D., Grosenbach, D., Hruby, D.E., Andrei, G., Blasco, R., Meyer, H., Snoeck, R., 2015. ST-246 is a key antiviral to inhibit the viral F13L phospholipase, one of the essential proteins for orthopoxvirus wrapping. J. Antimicrob. Chemother. 70, 1367–1380.

Edghill-Smith, Y., Golding, H., Manischewitz, J., King, L.R., Scott, D., Bray, M., Nalca, A., Hooper, J.W., Whitehouse, C.A., Schmitz, J.E., Reimann, K.A., Franchini, G., 2005. Smallpox vaccine–induced antibodies are necessary and sufficient for protection against monkeypox virus. Nat. Med. 11, 740–747.

Estupiñán, H.Y., Berglöf, A., Zain, R., Smith, C.I.E., 2021. Comparative analysis of BTK inhibitors and mechanisms underlying adverse effects. Front. Cell Dev. Biol. 9, 630942.

Fang, D., Liu, Y., Dou, D., Su, B., 2024. The unique immune evasion mechanisms of the mpox virus and their implication for developing new vaccines and immunotherapies. Virol. Sin. 39, 709–718.

Fluckiger, A.-C., Li, Z., Kato, R.M., Wahl, M.I., Ochs, H.D., Longnecker, R., Kinet, J.-P., Witte, O.N., Scharenberg, A.M., Rawlings, D.J., 1998. Btk/Tec kinases regulate sustained increases in intracellular Ca2+ following B-cell receptor activation. EMBO J. 17, 1973–1985.

Foster, S.A., Parker, S., Lanier, R., 2017. The role of brincidofovir in preparation for a potential smallpox outbreak. Viruses 9, 320.

Frischknecht, F., Moreau, V., Röttger, S., Gonfloni, S., Reckmann, I., Superti-Furga, G., Way, M., 1999. Actin-based motility of vaccinia virus mimics receptor tyrosine kinase signalling. Nature 401, 926–929.

Gilchuk, I., Gilchuk, P., Sapparapu, G., Lampley, R., Singh, V., Kose, N., Blum, D.L., Hughes, L.J., Satheshkumar, P.S., Townsend, M.B., Kondas, A.V., Reed, Z., Weiner, Z., Olson, V.A., Hammarlund, E., Raue, H.-P., Slifka, M.K., Slaughter, J.C., Graham, B.S., Edwards, K.M., Eisenberg, R.J., Cohen, G.H., Joyce, S., Crowe, J.E., 2016. Cross-Neutralizing and protective human antibody specificities to poxvirus infections. Cell 167, 684–694.e9.

Hajjo, R., Sabbah, D.A., Abusara, O.H., Kharmah, R., Bardaweel, S., 2023. Targeting human proteins for antiviral drug discovery and repurposing efforts: a focus on protein kinases. Viruses 15, 568.

Jefferies, C.A., Doyle, S., Brunner, C., Dunne, A., Brint, E., Wietek, C., Walch, E., Wirth, T., O'Neill, L.A.J., 2003. Bruton's tyrosine kinase is a Toll/Interleukin-1 receptor domain-binding protein that participates in nuclear factor κB activation by toll-like receptor 4. J. Biol. Chem. 278, 26258–26264.

Kang, Y., Gao, P., Chen, X., Zhai, X., Wang, X., Han, X., Jia, B., Hou, B., Zhou, X., Song, J., Zhang, F., 2025. *Lrrk2* promotes M1 macrophage polarization *via* regulating cytokine (IFN-γ) and TLR4 (LPS)-mediated responses. hLife 3, 98–111.

Karim, M., Lo, C.-W., Einav, S., 2023. Preparing for the next viral threat with broad-spectrum antivirals. J. Clin. Investig. 133, e170236.

Keating, J.A., Striker, R., 2012. Phosphorylation events during viral infections provide potential therapeutic targets. Rev. Med. Virol. 22, 166–181.

Langhammer, S., Koban, R., Yue, C., Ellerbrok, H., 2011. Inhibition of poxvirus spreading by the anti-tumor drug Gefitinib (Iressa). Antivir. Res. 89, 64–70.

Lee, K.-G., Xu, S., Kang, Z.-H., Huo, J., Huang, M., Liu, D., Takeuchi, O., Akira, S., Lam, K.-P., 2012. Bruton's tyrosine kinase phosphorylates toll-like receptor 3 to initiate antiviral response. Proc. Natl. Acad. Sci. U. S. A. 109, 5791–5796.

Lin, Y., Hu, Z., Fu, Y.-X., Peng, H., 2024. Mucosal vaccine development for respiratory viral infections. hLife 2, 50–63.

Matía, A., Lorenzo, M.M., Romero-Estremera, Y.C., Sánchez-Puig, J.M., Zaballos, A., Blasco, R., 2022. Identification of β2 microglobulin, the product of B2M gene, as a Host Factor for Vaccinia Virus Infection by Genome-Wide CRISPR genetic screens. PLoS Pathog. 18, e1010800.

Mercer, J., Knébel, S., Schmidt, F.I., Crouse, J., Burkard, C., Helenius, A., 2010. Vaccinia virus strains use distinct forms of macropinocytosis for host-cell entry. Proc. Natl. Acad. Sci. U. S. A. 107, 9346–9351.

Minhaj, F.S., 2022. Orthopoxvirus testing challenges for persons in populations at low risk or without known epidemiologic link to monkeypox — united States, 2022. MMWR Morb. Mortal. Wkly. Rep. 71, 1155–1158.

Mitjà, O., Ogoina, D., Titanji, B.K., Galvan, C., Muyembe, J.-J., Marks, M., Orkin, C.M., 2023. Monkeypox. Lancet 401, 60–74.

Ndembi, N., Folayan, M.O., Komakech, A., Mercy, K., Tessema, S., Mbala-Kingebeni, P., Ngandu, C., Ngongo, N., Kaseya, J., Abdool Karim, S.S., 2025. Evolving Epidemiology of Mpox in Africa in 2024. N. Engl. J. Med. 392, 666–676.

Newsome, T.P., Weisswange, I., Frischknecht, F., Way, M., 2006. Abl collaborates with Src family kinases to stimulate actin-based motility of vaccinia virus. Cell. Microbiol. 8, 233–241.

Niu, K., Wang, X., Jiang, Q., Liu, K., Xie, S., Song, B., Wu, W., Li, X., Peng, C., 2025. Ibrutinib inhibits the replication of multiple poxviruses by targeting the Bruton tyrosine kinase. J. Virol. 99, e00517-25.

Peng, C., Zhou, Y., Cao, S., Pant, A., Campos Guerrero, M.L., McDonald, P., Roy, A., Yang, Z., 2020. Identification of Vaccinia Virus inhibitors and cellular functions necessary for efficient viral replication by screening bioactives and FDA-Approved drugs. Vaccines 8, 401.

Pérez-García, J.-A., Dans-Vilan, L., Montero-Morales, L., Culebras, E., Fernández-Castelao, S., Miguel-Benito, Á., Puerta-López, T., Delgado-Iribarren García-Campero, A., 2026. First case of Mpox clade Ib transmitted from human-to-human outside the African continent and not linked to travel. Int. J. Infect. Dis. 163, 108224.

Reeves, P.M., Bommarius, B., Lebeis, S., McNulty, S., Christensen, J., Swimm, A., Chahroudi, A., Chavan, R., Feinberg, M.B., Veach, D., Bornmann, W., Sherman, M., Kalman, D., 2005. Disabling poxvirus pathogenesis by inhibition of Abl-family tyrosine kinases. Nat Med 11, 731–739.

Reeves, P.M., Smith, S.K., Olson, V.A., Thorne, S.H., Bornmann, W., Damon, I.K., Kalman, D., 2011. Variola and monkeypox viruses utilize conserved mechanisms of virion motility and release that depend on abl and SRC family tyrosine kinases. J. Virol. 85, 21–31.

Ren, W., Lan, J., Ju, X., Gong, M., Long, Q., Zhu, Z., Yu, Y., Wu, J., Zhong, J., Zhang, R., Fan, S., Zhong, G., Huang, A., Wang, X., Ding, Q., 2021. Mutation Y453F in the Spike Protein of SARS-CoV-2 Enhances Interaction with the Mink ACE2 Receptor for Host Adaption. PLoS Pathog. 17, e1010053.

Ritter, J.M., Martines, R.B., Bhatnagar, J., Rao, A.K., Villalba, J.A., Silva-Flannery, L., Lee, E., Bullock, H.A., Hutson, C.L., Cederroth, T., Harris, C.K., Hord, K., Xu, Y., Brown, C.A., Guccione, J.P., Miller, M., Paddock, C.D., Reagan-Steiner, S., Mpox Pathology Working Group, 2024. Pathology and monkeypox virus localization in tissues from immunocompromised patients with severe or fatal mpox. J. Infect. Dis. 229, S219–S228.

Roschewski, M., Lionakis, M.S., Sharman, J.P., Roswarski, J., Goy, A., Monticelli, M.A., Roshon, M., Wrzesinski, S.H., Desai, J.V., Zarakas, M.A., Collen, J., Rose, K.M., Hamdy, A., Izumi, R., Wright, G.W., Chung, K.K., Baselga, J., Staudt, L.M., Wilson, W.H., 2020. Inhibition of Bruton tyrosine kinase in patients with severe COVID-19. Sci. Immunol. 5, eabd0110.

Sanjana, N.E., Shalem, O., Zhang, F., 2014. Improved vectors and genome-wide libraries for CRISPR screening. Nat. Methods 11, 783–784.

Shaw, M.L., 2020. Second-generation BTK inhibitors hit the treatment bullseye with fewer off-target effects. Am J Manag Care 26, SP226–SP227.

Smith, T.G., Gigante, C.M., Wynn, N.T., Matheny, A., Davidson, W., Yang, Y., Condori, R. E., O'Connell, K., Kovar, L., Williams, T.L., Yu, Y.C., Petersen, B.W., Baird, N., Lowe, D., Li, Y., Satheshkumar, P.S., Hutson, C.L., 2023. Tecovirimat Resistance in Mpox Patients, United States, 2022–2023. Emerg. Infect. Dis. 29, 2426–2432.

Tasso, B., Spallarossa, A., Russo, E., Brullo, C., 2021. The development of BTK inhibitors: a five-year update. Molecules 26, 7411.

Taylor, L., 2025. WHO Declares Mpox Emergency over but Says Threat Remains. BMJ (Clinical research ed.), 390, r1908.

The PALM007 Writing Group, 2025. Tecovirimat for clade I MPXV infection in the Democratic Republic of Congo. N. Engl. J. Med. 392, 1484–1496.

Titanji, B.K., Hazra, A., Zucker, J., 2024. Mpox clinical presentation, diagnostic approaches, and treatment strategies: a review. JAMA 332, 1652–1662.

Tiwari, A., Kalonji, T., Miller, T., Van Den Bossche, T., Krolicka, A., Muhindo-Mavoko, H., Mitashi, P., Tahita, M.C., Lood, R., Pitkänen, T., Maketa, V., 2025. Emergence and global spread of mpox clade ib: challenges and the role of wastewater and environmental surveillance. J. Infect. Dis. 231, e825–e829.

Treon, S.P., Castillo, J.J., Skarbnik, A.P., Soumerai, J.D., Ghobrial, I.M., Guerrera, M.L., Meid, K., Yang, G., 2020. The BTK inhibitor ibrutinib may protect against pulmonary injury in COVID-19–infected patients. Blood 135, 1912–1915.

Vakaniaki, E.H., Kacita, C., Kinganda-Lusamaki, E., O'Toole, Á., Wawina-Bokalanga, T., Mukadi-Bamuleka, D., Amuri-Aziza, A., Malyamungu-Bubala, N., Mweshi-Kumbana, F., Mutimbwa-Mambo, L., Belesi-Siangoli, F., Mujula, Y., Parker, E., Muswamba-Kayembe, P.-C., Nundu, S.S., Lushima, R.S., Makangara-Cigolo, J.-C., Mulopo-Mukanya, N., Pukuta-Simbu, E., Akil-Bandali, P., Kavunga, H., Abdramane, O., Brosius, I., Bangwen, E., Vercauteren, K., Sam-Agudu, N.A., Mills, E. J., Tshiani-Mbaya, O., Hoff, N.A., Rimoin, A.W., Hensley, L.E., Kindrachuk, J., Baxter, C., de Oliveira, T., Ayouba, A., Peeters, M., Delaporte, E., Ahuka-Mundeke, S., Mohr, E.L., Sullivan, N.J., Muyembe-Tamfum, J.-J., Nachega, J.B., Rambaut, A., Liesenborghs, L., Mbala-Kingebeni, P., 2024. Sustained human outbreak of a new MPXV clade I lineage in eastern Democratic Republic of the Congo. Nat Med 30, 2791–2795.

Wang, L., Zhang, T., Wang, N., Liu, X., Kang, D., 2026. Recent progress in the discovery of anti-mpox agents. Med. Res. Rev. 46, 40–69.

Wu, S., Deng, J., Du, M., Liu, M., Liu, J., 2025. Global transmission characteristics of mpox outbreaks: a systematic review and meta-analysis. EClinicalMedicine 89, 103526.

Yang, C., Yu, Y., Peng, Q., Song, J., Sun, B., Shi, Y., Ding, Q., 2024. Drupacine as a potent SARS-CoV-2 replication inhibitor *in vitro*. Biosafety and Health 6, 270–278.

Yang, G., Pevear, D.C., Davies, M.H., Collett, M.S., Bailey, T., Rippen, S., Barone, L., Burns, C., Rhodes, G., Tohan, S., Huggins, J.W., Baker, R.O., Buller, R.L.M., Touchette, E., Waller, K., Schriewer, J., Neyts, J., DeClercq, E., Jones, K., Hruby, D., Jordan, R., 2005. An orally bioavailable antipoxvirus compound (ST-246) inhibits extracellular virus Formation and protects mice from lethal Orthopoxvirus challenge. J. Virol. 79, 13139–13149.

Young, L., Sung, J., Stacey, G., Masters, J.R., 2010. Detection of Mycoplasma in cell cultures. Nat. Protoc. 5, 929–934.

Zhang, J.-H., Chung, T.D.Y., Oldenburg, K.R., 1999. A simple statistical parameter for use in evaluation and validation of high throughput screening assays. SLAS Discovery 4, 67–73.

Zhao, R., Wu, L., Sun, J., Liu, D., Han, P., Gao, Y., Zhang, Y., Xu, Y., Qu, X., Wang, H., Chai, Y., Chen, Z., Gao, G.F., Wang, Q., 2024. Two noncompeting human neutralizing antibodies targeting MPXV B6 show protective effects against orthopoxvirus infections. Nat. Commun. 15, 4660.

Zhu, W., Fang, Q., Zhuang, K., Wang, H., Yu, W., Zhou, J., Liu, L., Tien, P., Zhang, L., Chen, Z., 2007. The attenuation of vaccinia Tian Tan strain by the removal of the viral M1L-K2L genes. J. Virol. Methods 144, 17–26.

Zhu, Z., Han, Y., Gong, M., Sun, B., Zhang, R., Ding, Q., 2024. Establishment of replication-competent vesicular stomatitis virus recapitulating SADS-CoV entry. J. Virol. 98, e01957-23.

Zucker, J., Fischer, W.A., Zheng, L., McCarthy, C., Saha, P.T., Javan, A.C., Greninger, A., Hamill, M.M., Leslie, K., Brooks, K.M., Berardi, J., Smith, D., Hosey, L., Aldrovandi, G., Ferbas, K., Day, C., Ignacio, R.A.B., Bolan, R., Glesby, M.J., Landovitz, R.J., Luetkemeyer, A.F., Madero, J.S., Gandhi, R.T., Nachman, S., Eron, J., Currier, J.S., Wilkin, T., 2026. Tecovirimat for the treatment of mpox. N. Engl. J. Med. 394, 884–895.